Investigation of CO_2 adsorption on amine-functionalized silicas and metal-organic polymers

N. A. Mamonov, S. A. Mikhailov, G. E. Dzhungurova, A. E. Bessudnov, D. A. Grigor´ev, I. M. Bedrina, and M. N. Mikhailov★

LLC "RN-RDC",
Build. 2, 55/1 Leninsky prosp., 119333 Moscow, Russian Federation.
Fax: +7 (495) 730 6101. E-mail: MikhailovMN@rn-rdc.ru

Adsorption properties of amine-functionalized mesoporous silica NH_2-SBA-15, zeolite-like imidazole framework ZIF-8, and amine-functionalized metal-organic polymer NH_2-MIL-53 have been investigated. Non-modified mesoporous adsorbent SBA-15 has a higher sorption capacity for CO_2 than microporous ZIF-8, although microporous sample is characterized by a larger surface area and the values of total pore volume are close. When amine groups are present on the surface of the adsorbents, the chemical adsorption contributes more then the physical one. The adsorption capacity increases with increasing concentration of the functional groups which, in its turn, correlates with adsorbent surface area. Among the studied samples, the best adsorption properties demonstrate amine-functionalized adsorbents, amine-functionalized mesoporous silica NH_2-SBA-15, and amine-functionalized metal-organic polymer NH_2-MIL-53.

Key words: adsorbent, amine-functionalized silica, flue gases, carbon dioxide, metal-organic polymer, immobilized silica, zeolitic imidazole framework, metal-organic coordination frameworks.

Carbon dioxide is one of the anthropogenic gases, the contribution of which to the greenhouse effect approaches 65%. The main reason of the increased level of CO_2 in the atmosphere is fossil fuel combustion at the industrial processes.[1] A decrease in carbon dioxide emissions to the atmosphere could be achieved by sequestration of CO_2 from flue gases. Amine gas treating is the most popular industrial technology to remove CO_2 from the post-combustion flue gas streams. However, this method has a number of disadvantages, among which are the corrosive properties of amines, their limited sorption capacity, decomposition during the operation, high energy consumption in regeneration of amines, the need to maintain an increased pressure at absorption.[2,3] The technology of gas separation using adsorption method enables one to avoid these shortcomings. When using solid adsorbents, carbon dioxide sequestration becomes feasible under low CO_2 partial pressure, which significantly reduces energy consumption. In this case, the pressure of the flue gases is *ca.* 1 atm., the operating temperature is 40—130 °C, and the CO_2 concentration is 4—14%.[4]

To increase the adsorption of CO_2 at low partial pressure, selective adsorbents are required. Zeolites, amine-modified silicas, and metal-organic frameworks (MOF) are considerd to be appropriate.[5]

Among zeolites, 13X (NaX) molecular sieve characterized by the highest sorption capacity (~2 mmol g^{-1} at 1 atm.) is regarded as a prominent material for CO_2 adsorption.[6] Nevertheless, zeolites loose their efficiency at temperatures above 50 °C and in the presence of water.[7]

Amine-functionalized adsorbents are effectively capture CO_2 according to the following chemical reaction[8,9]

$$R{-}NH_2 + CO_2 \longrightarrow R{-}NH_2^+COO^- \longrightarrow R{-}NHCOOH.$$

Among amine-functionalized mesoporous silicas, NH_2-SBA-15 was indicated as the most appropriate material for the carbon dioxide removal.[10] Its high sorption capacity for CO_2 is associated with both chemical adsorption by the grafted amines and physical adsorption in mesopores.[11,12]

Metal-organic coordination frameworks (MOF) are materials with a high surface area, synthetically controlled size and form of pores, a possibility to introduce functional groups into the framework. In addition, an efficient CO_2 capture from the flue gases at low partial pressures (0.05—0.4 atm) was demonstrated. This behavior is common for the structures which contain amine groups, for example NH_2-MIL-53 metal-organic adsorbent,[13,14] as well as for non-functionalized structures such as zeolite-like imidazole frameworks (ZIF). ZIF structures are a class of MOF material which, among all, are stable in the pres-

Published in Russian in *Izvestiya Akademii Nauk. Seriya Khimicheskaya,* No. 9, pp. 1595—1600, September, 2018.
1066-5285/18/6709-1595

ence of water. Moreover, pore diameter of one of these adsorbents, ZIF-8, exceed the dimension of carbon dioxide molecule size which is favorable for efficient adsorption of CO_2.[15]

As a rule, comparative studies of various adsorbents in carbon dioxide removal from the flue gases were carried out within the same class of compounds.[16] Moreover, since various conditions were applied in experiments the comparison of the results is difficult. Accordingly, the goal of the present work was to compare the adsorption properties of the materials promising for the CO_2 capture. The comparison was conducted under conditions simulating the adsorption of carbon dioxide from the post-combustion flue gases (CO_2 concentration 5—15 vol.%, temperature 40 °C, partial pressure 0.05—0.4 atm.). ZIF-8, NH_2-MIL-53 and NH_2-SBA-15 have been selected as adsorbents, and the as-received mesoporous silica SBA-15 was used for comparison purposes.

Experimental

Synthesis of SBA-15. Mesoporous silica SBA-15 was synthesized using the protocol described earlier.[17] Copolymer Pluronic P123 (16 g) was dissolved in 120 g of distilled water and 480 g of 2 *M* solution of HCl with constant stirring at 35 °C. Then 45 g of tetraethylorthosilicate (TEOS) was added to the mixture and stirred for 20 h at 35 °C. The reactant ratio TEOS : HCl : H_2O : P123 in the mixture was 1 : 4.4 : 148 : 0.013. Then the reaction mixture was maintained at 100 °C for 12 h without stirring. The resulting product was filtrated, washed with distilled water and dried in the air at ~20 °C, then calcinated for 6 h at 550 °C.

Synthesis of NH_2-SBA-15. Amine-functionalized silica was prepared by the known method.[18] SBA-15 silica (15 g) in 250 mL of toluene was stirred for 30 min, then 50 mL of 3-aminopropyltriethoxysilane was added and the mixture was stored for 16 h at 100 °C. A reflux condenser was used to avoid evaporation. The resulting product, NH_2-SBA-15, was filtered, washed with ethanol (250 mL), then dried for 12 h at 60 °C.

Synthesis of ZIF-8. Zeolite-like imidazole frameworks ZIF-8 was synthesized using the procedure similar to that described earlier.[19] 2-Methylimidazole (3.312 g, 40.43 mmol) was dissolved in distilled water (48 mL) and 2 mL (14 mmol) of triethylamine was added. Another solution contained $Zn(NO_3)_2 \cdot 6H_2O$ (2 g, 6.72 mmol) dissolved in 12 mL of water. Then both solutions were mixed and this reaction mixture was vigorously stirred for 0.5 h at ~20 °C. The residue was filtrated, washed several times with distilled water (150 mL). The obtained substance was dried for 12 h at 60 °C and then refluxed for 12 h in 25 mL of methanol. The product was filtered and dried for 2 h in vacuum drying oven at 200 °C ($6 \cdot 10^{-6}$ atm.).

Synthesis of NH_2-MIL-53. Amine-functionalized metal-organic polymer was obtained using the earlier described procedure.[20] Solutions of anhydrous alumina nitrate $Al(NO_3)_3$ (0.788 g, 2.10 mmol) in 15 mL of DMF and of 2-aminetereftolate acid (0.565 g, 3.12 mmol) in 15 mL of DMF were mixed in Teflone autoclave and stored for 3 days at 130 °C. The obtained yellowish gel was filtrated and washed with acetone, after which was dried in air. Solid product was placed in methanol and boiled at 65 °C using the reflux condenser. Then the substance was filtered, washed in methanol and dried for 8 h at 110°C ($6 \cdot 10^{-6}$ atm.) in vacuum drying oven.

Characterization of adsorbents. X-ray diffraction analysis was performed on a PhilipsX´PertPROMPD difractometer using Cu-Kα-radiation and a scanning rate of 2.0 deg min^{-1}

Investigation of the samples by transition electron microscopy was carried out using a JEOLJEM 2100 FUHR/Cs microscope. The instrument was equipped with a spherical aberration (Cs) corrector and a characteristic X-ray detector capable of collecting XRD data in the energy range of 0.5—30 keV. Tungsten cathode coated with zirconium dioxide ZrO_2 was used as an electron source; the accelerating voltage was 200 kV. Dark field images were obtained using the scanning mode (SPEM). Sample preparation included dispersing a weighted sample (0.5—1 mg) in 1—1.5 mL of ethanol or distilled water by ultrasonic treatment in a Sapphire Ultra-Lite ultrasonic bath (LLC NPO Sapphire) for 5—15 min, after which a drop of the resulting suspension was placed on a copper grid with a polymer microfine film support (Fomvar, AgarScientific) coated with an amorphous carbon layer.

The spectra of energy dispersive X-ray microstructure analysis (RSMA) were recorded using an EDS attachment on a JEOL JSM-6390LA scanning electron microscope (JEOL Ltd., Japan). The sample was supported on a double-sided carbon electroconductive tape stuck on a copper-zinc table. Then the table with a sample was placed in a microscope chamber and evacuated to a pressure of 10^{-4} Pa. Accelerating voltage was 20 kV at a working distance of 25 mm.

Low-temperature nitrogen adsorption/desorption isotherms were measured at −196 °C using an ASAP 2020 (Micromeritics) instrument. The surface area of the samples was calculated on the basis of the linear form of the Brunauer-Emmett-Teller equation (BET), assuming that the surface area of the nitrogen molecule is $16.2 \cdot 10^{-20}$ m^2. The total pore volume was evaluated by nitrogen adsorption measured at a relative pressure $p/p_0 = 0.99$. The values of the total pore volume were obtained by combining the volumes of micropores, mesopores and macropores.

The nitrogen content of the adsorbents was determined by an ICP 61 atomic emission spectrometer (Termo Jarrell Ash).

The diffuse reflection infrared spectra (DRIFTS) were recorded at ~20 °C on a Nicoleti S50 spectrometer (Thermo Fisher Scientific) equipped with a Praying Mantis diffuse reflection attachment (Harrick Scientific Products, Inc.) with a high-temperature reaction chamber. The spectra were collected in the range of 4000—400 cm^{-1} at a resolution of 4 cm^{-1}. The background in the DRIFTS geometry was measured with respect to KBr powder. Before measuring the spectra, a powder sample was evacuated at 100 °C for 0.5 h to remove physically adsorbed gases and water.

Measurements of the static adsorption capacity The static adsorption capacity for CO_2 was determined using an Autosorb iQ multifunctional sorption system (Quantachrome Instruments) at a constant temperature of 40 °C. Adsorption isotherms were obtained at several CO_2 pressures in the range from 0 to 1 atm. Before recording the isotherms, samples were degassed in a vacuum.

Measurements of the dynamic capacity of the adsorbent. The dynamic adsorption capacity for CO_2 was determined using a Cirrus 2 quadrupole mass spectrometer (Micromeritics), fixing the time of protective action of the adsorbent bed. A weighted

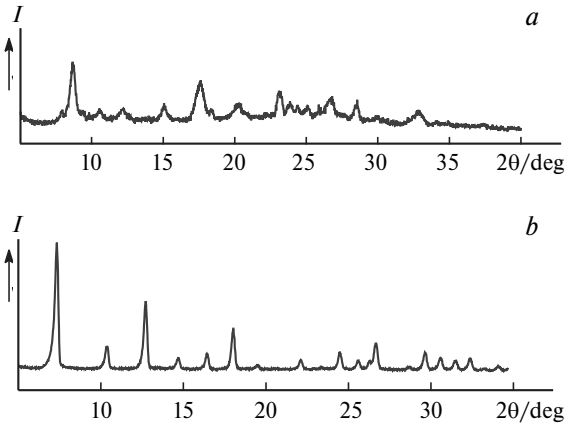

Fig. 1. XRD pattern of the synthesized ZIF-8 (*a*) and NH_2-MIL-53 (*b*).

sample (0.1 g) was placed into a quartz U-shaped chemisorption analyzer reactor AutoChem II 2920 (Micromeritics). Before the measurements, the reactor with loaded sample was purged for 1 hour in a He flow at 120 °C and then cooled down to the adsorption temperature (40 °C). Adsorption of CO_2 was carried out using a 5%CO_2/He (vol/vol) gas flow at a rate of 3—5 mL min^{-1} until the sample was completely saturated at atmospheric pressure. The protective action time of the adsorbent bed was determined as a temporal interval from the moment of the adsorption starts to the moment at which the initial concentration of CO_2 in the mixture was equal to the amount of CO_2 in the gas flow at the outlet of the reactor.

Results and Discussion

Physicochemical properties of the studied adsorbents. To confirm the phase homogeneity of the synthesized adsorbents, metal-organic polymers ZIF-8 and NH_2-MIL-53 were studied by XRD (Fig. 1).

The XRD pattern of ZIF-8 (see Fig. 1, *a*) shows strong peaks at 2θ = 7.3, 10.4, 12.7 and 18.1°, corresponding to reflections from the (011), (002), (112), and (222) planes of ZIF-8 structure.[21] The XRD pattern of NH_2-MIL-53 (see Fig. 1, *b*) contains characteristic peaks at 2θ = 9.0° (110) and 18.0° (double signals from (211) and (220) planes).[22]

To confirm the phase composition of NH_2-SBA-15, which has X-ray amorphous silica microstructure, SPEM was used. Figure 2 shows the dark-field image of NH_2-SBA-15; rectangles are the areas used to record X-ray energy-dispersive spectra. The SPEM data indicate the presence of an ordered mesoporous structure, characteristic of SBA-15, formed by direct separate pores. The results of the RSMA confirm that the sample includes silicon and oxygen, they provide evidence of the absence of impurities, and also indicate the presence of elemental nitrogen in the mesopores.

The results of chemical modification of the initial mesoporous SBA-15 silica with aminosilane were investigated by IR spectroscopy. Figure 3 shows the diffuse reflection IR spectra of mesoporous SBA-15 silica and NH_2-SBA-15 adsorbent at 25 °C in the region 3800—2600 cm^{-1}.

According to the current understanding of the process of modification of mesoporous silicas with aminosilanes,[23,24] surface functionalization occurs owing to the reaction of aminosilane with OH groups on the silica surface. When comparing the spectra of the initial and modified samples, one can see that in the spectrum of NH_2-SBA-15, *i.e.* after functionalization, there are absorption bands at 3372 and 3304 cm^{-1} ascribed to asymmetric

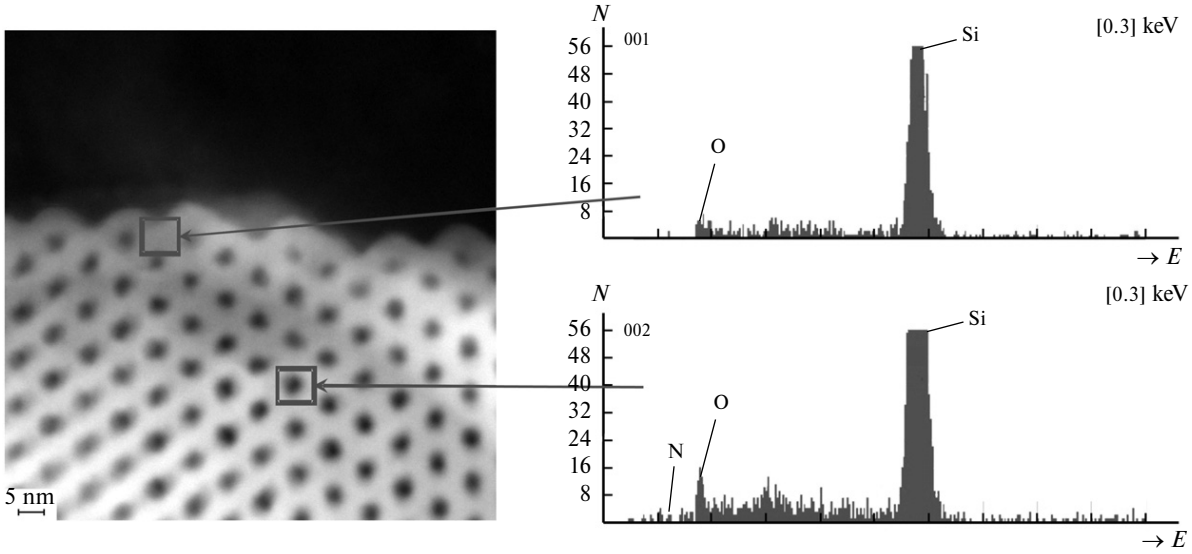

Fig. 2. Dark field SPEM image with the selected area and the spectra of X-ray microstructured analysis (RSMA) for these areas; *N* is the number of the registered impulses, *E* is the energy of electron emission.

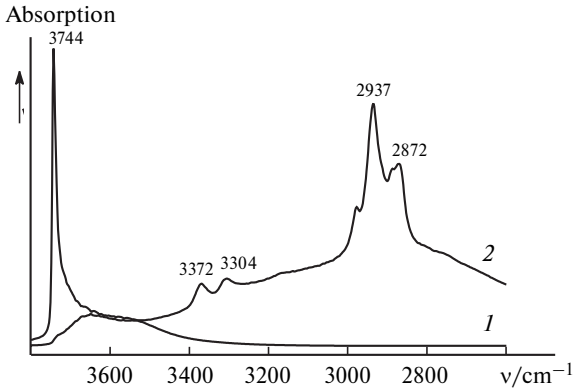

Fig. 3. IR spectra of SBA-15 (*1*) and NH_2-SBA-15 (*2*).

and symmetric NH_2 vibrations, respectively, and the bands at 2872 and 2937 cm^{-1} typical of stretching CH_2-vibrations. In the spectrum of the modified sample, NH_2-SBA-15, the band at 3744 cm^{-1} corresponding to the silanol OH groups disappears indicating that the reaction of the aminosilane agent with the hydroxy groups of mesoporous silica was successfully accomplished. By comparing the data obtained by SPEM and DRIFTS methods, it can be inferred that the mesoporous structure persists during amine treatment and the degree of coverage of the initial silica with the modifying agent is very high.

It is well known that the structure and porosity of adsorbents affects their adsorption capacity.[25] The mechanism of the internal diffusion depends on the pore size. The presence of mesopores in the adsorbent enhances the adsorption capacity of the material as well as increases the diffusion rate.[26,27] In order to determine the structural characteristics, the samples were investigated by nitrogen porosimetry. Figure 4 shows nitrogen adsorption-desorption isotherms recorded for selected adsorbents and mesoporous silica SBA-15.

Figure 4 shows that in ZIF-8 and NH_2-MIL-53 samples, pores are filled in the low-pressure region. This indicates that the main volume of adsorption space is occupied by micropores.[21,22] The capillary-condensation hysteresis loops on the curves obtained for the samples SBA-15 and NH_2-SBA-15 indicate the presence of through-hole cylindrical mesopores in the adsorbents,[28] and similar shape of the loops suggests that the structure of the initial mesoporous silica SBA-15 was not affected by the introduction of amino groups.

The structural characteristics of the sy nthesized adsorbents are summarized in Table 1.

Study of CO_2 adsorption. Adsorption properties of the synthesized samples were estimated by measuring statical and dynamic adsorption capacity.

The isotherms of CO_2 adsorption recorded at 40 °C and in the pressure range 0—1 atm. for SBA-15, NH_2-SBA-15, ZIF-8, and NH_2-MIL-53, are given in Fig. 5.

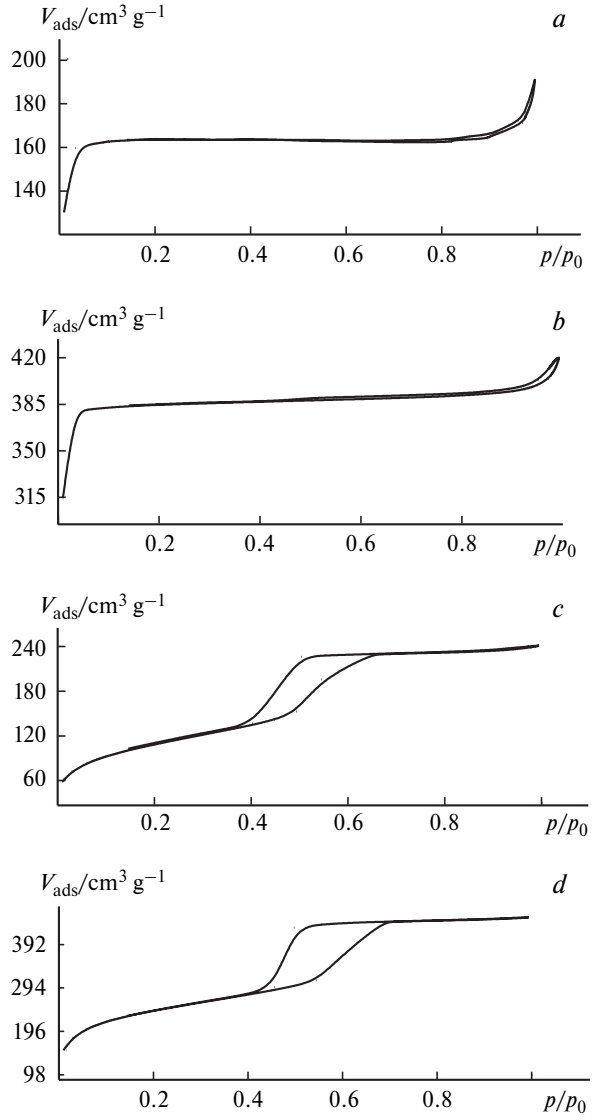

Fig. 4. Adsorption—desorption of nitrogen on NH_2-MIL-53 (*a*), ZIF-8 (*b*), NH_2-SBA-15 (*c*), and SBA-15 (*d*) adsorbents.

The highest adsorption capacity was observed for NH_2-MIL-53 (see Fig. 5, curve *4*) and NH_2-SBA-15 (see Fig. 5, curve *2*). At pressure of CO_2 from 0.1 to 0.4 atm., their adsorption capacity was 0.7—1.7 mmol g^{-1}. Adsorption

Table 1. Surface area (*S*) calculated by BET and pore volume (*V*) of SBA-15, NH_2-SBA-15, ZIF-8, and NH_2-MIL-53 adsorbents

Adsorbent	S/m^2 g^{-1}	V/cm^3 g^{-1}		
		total	micropore	mesopore
SBA-15	855	0.62	0	0.62
NH_2-SBA-15	417	0.41	0	0.41
ZIF-8	1280	0.63	0.58	0.05
NH_2-MIL-53	683	0.34	0.25	0.09

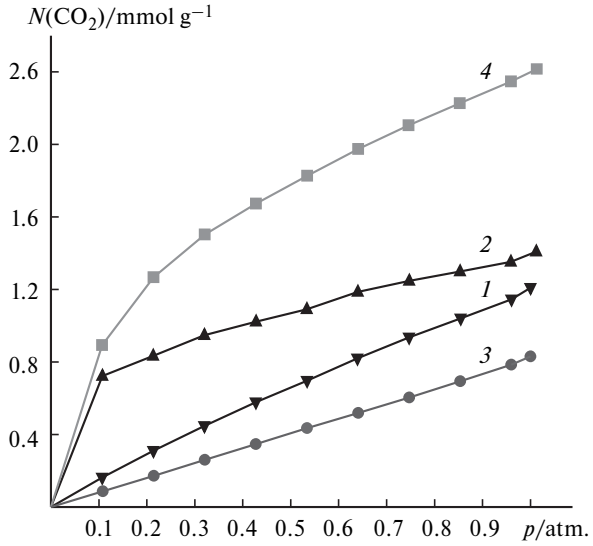

Fig. 5. Isotherm of CO_2 adsorption on SBA-15 (*1*), NH_2-SBA-15 (*2*), ZIF-8 (*3*), and NH_2-MIL-53 (*4*).

isotherms of SBA-15 and ZIF-8 (see Fig. 5, curves *1* and *3*) are linear over the pressure range 0—1 atm. At the same time, the adsorption isotherm curve of mesoporous silica lies above other curves over the entire pressure range. This behavior indicates a higher adsorption capacity of mesoporous silica compared to ZIF-8, which is explained by the large volume of mesopores (see Table 1).

The experiments on CO_2 adsorption under dynamic conditions (1 atm., 40 °C) were conducted to determine the time of protective action of the adsorbents; hence, the dynamic capacity of the samples was studied. Figure 6 shows the dependence of the volume fraction of CO_2 in the flow gas mixture (5%CO_2/He) on the time of the gas flow through the layer of adsorbent.

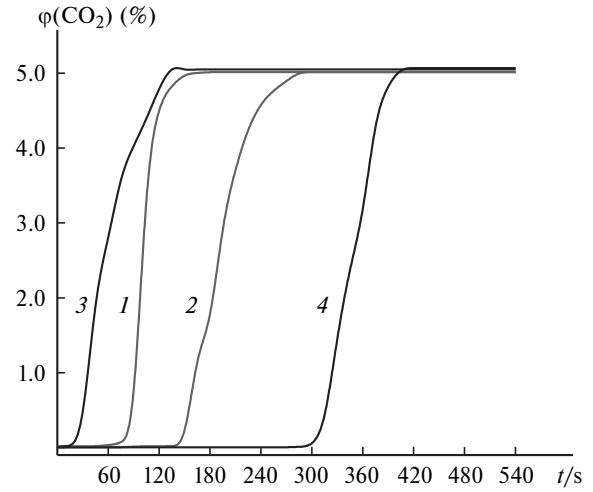

Fig. 6. Volume fraction of CO_2 (φ(CO_2)) in gas flow (5%CO_2/He, 1 atm., 40 °C) as a function of consumption time for SBA-15 (*1*), NH_2-SBA-15 (*2*), ZIF-8 (*3*), and NH_2-MIL-53 (*4*).

Table 2. The values of static (I) and dynamic (II) adsorption capacity (*A*) and the time of protecting action of SBA-15, NH_2-SBA-15, ZIF-8, and NH_2-MIL-53 adsorbents

Adsorbent	[NH_2]* /mmol g^{-1}	*A*/mmol g^{-1}		*t*/s
		I	II	
SBA-15	—	0.22	0.24	60
NH_2-SBA-15	2.5	0.77	0.51	140
ZIF-8	—	0.13	0.18	25
NH_2-MIL-53	4.3	1.05	0.62	275

* Concentration of NH_2-group in the sample.

The values of the static adsorption capacity of the studied adsorbents at CO_2 pressure of 0.15 atm., which corresponds to the average partial pressure of CO_2 in the flue gas, are given in Table 2. The Table is also complemented with the values of the dynamic adsorption capacity and the protective action time of these samples.

The static adsorption capacity of the SBA-15 sample (0.22 mmol g^{-1}) is higher than that of the ZIF-8 adsorbent (0.13 mmol g^{-1}), due to a higher mesopore volume of SBA-15 (see Table 1). A larger volume of mesopores contributes to an increase in the proportion of physically adsorbed carbon dioxide molecules, which increases the protective action time of SBA-15 (from 25 to 60 s) and its dynamic adsorption capacity.

Amine-functionalized samples are three times more effective than the non-modified adsorbents in terms of the static adsorption capacity and show two-folds improvement in dynamic adsorption. This fact evidences a greater contribution of the chemical adsorption compared to the physical adsorption of amine-modified samples NH_2-SBA-15 and NH_2-MIL-53.

The surface concentration of amine groups in the amine-functionalized samples NH_2-SBA-15 and NH_2-MIL-53 is different: 2.5 and 4.3 mmol g^{-1}, respectively. A higher concentration of NH_2-groups, characteristic of the functionalized MOF, enhances CO_2 adsorption. At the same time, concentration of the functional groups (see Table 2) linearly correlates with the surface area of the samples (see Table 1). However, the mesoporous structure of NH_2-SBA-15 makes it possible to increase the capacity of the sample due to physical adsorption. Thus, at a ratio of NH_2-group concentrations for samples of NH_2-MIL-53/NH_2-SBA-15 of 1.7, the ratio of their static adsorption capacity for CO_2 is 1.4 and that of dynamic adsorption capacity is 1.2.

To sum up, a comparative study of the adsorption properties of promising materials for the CO_2 capture from the flue gases has shown that the presence of mesopores positively affects the adsorption capacity owing to the contribution of the physical adsorption. However, in the case of the surface functionalization of adsorbents, in particular amine grafting, the chemical adsorption con-

tributes much more to the adsorption capacity than the physical one. Moreover, the adsorption capacity increases with increasing concentration of the functional groups, which in its turn is proportional to the surface area of the adsorbents.

Among the adsorbents studied, amine-modified samples, i.e. amine-functionalized mesoporous silica NH_2-SBA-15 and metal-organic adsorbent NH_2-MIL-53, are characterized with improved adsorption properties: the static adsorption capacity is 0.77 and 1.05 mmol g^{-1}, respectively, and dynamic adsorption capacity is 0.51 and 0.62 mmol g^{-1}.

References

1. N. Du, H. B. Park, M. M. Dal-Cin, M. D. Guiver, *Energy Environ. Sci.*, 2012, **5**, 7306—7322.
2. E. S. Rubin, *Elements*, 2008, **4**, 311—317.
3. E. S. Rubin, C. Chen, A. B. Rao, *Energy Policy*, 2007, **35**, 4444—4454.
4. X. Luo, M. Wang, J. Chen, *Fuel*, 2015, **151**, 110—117.
5. Z. H. Lee, K. T. Lee, S. Bhatia, A. R. Mohamed, *Renewable and Sustainable Energy Reviews*, 2012, **16**, 2599—2609.
6. G. Calleja, J. Pau, J. A. Calles, *J. Chem. Eng. Data*, 1998, **43**, 994—1000.
7. J. S. Lee, J. H. Kim, J. T. Kim, J. K. Suh, J. M. Lee, C. H. Lee, *Chem. Eng. Data*, 2002, **47**, 1237—1242.
8. A. Sayari, Y. Belmabkhout, *J. Am. Chem. Soc.*, 2010, **132**, 6312—6314.
9. J. J. Lee, C.-H. Chen, D. Shimon, S. E. Hayes, C. Sievers, C. W. Jones, *J. Phys. Chem. C*, 2017, **121**, 23480—23487.
10. A. Samanta, A. Zhao, G. K. H. Shimizu, P. Sarkar, P. Gupta, *Ind. Eng. Chem. Res.*, 2012, **51**, 1438—1463.
11. V. Zelenak, M. Badanicova, D. Halamova, J. Cejka, A. Zukal, N. Murafa, G. Goerigk, *J. Chem. Eng.*, 2008, **144**, 336—347.
12. N. Rao, M. Wang, Z. Shang, Y. Hou, G. Fan, J. Li, *Energy Fuels*, 2018, **32**, 670—677.
13. B. Arstad, H. Fjellvag, K. O. Kongshaug, O. Swang, R. Blom, *Adsorption*, 2008, **14**, 755—762.
14. H. R. Abid, Z. H. Rada, X. Duan, H. Sun, S. Wang, *Energy Fuels*, 2018, **32**, 4502—4510; DOI: 10.1021/acs.energyfuels.7b03240.
15. L. S. Lai, Y. F. Yeong, N. C. Ani, K. K. Lau, A. M. Shariff, *Particulate Sci. Technol.*, 2014, **32**, 520—528.
16. J.-R. Li, Y. Ma, M. C. McCarthy, J. Sculley, J. Yu, H.-K. Jeong, P. B. Balbuena, H.-C.Zhou, *Coord. Chem. Rev.*, 2011, **255**, 1791—1800.
17. D. Zhao, Q. Huo, J. Feng, B. F. Chmelka, G. D. Stucky, *J. Am. Chem. Soc.*, 1998, **120**, 6024—3036.
18. W. Klinthong, K. Chao, C. Tan, *Ind. Eng. Chem. Res.*, 2013, **52**, 9834—9842.
19. N. A. H. M. Nordin, A. F. Ismail, A. Mustafa, P. S. Goh, D. Rana, T. Matsuura, *RSC Adv.*, 2014, **4**, 33292—33300.
20. S. Couck, J. F. M. Denayer, G. V. Baron, T. Remy, J. Gascon, F. Kapteijn, *J. Am. Chem. Soc.*, 2009, **131**, 6326—6327.
21. X. Liu, Y. Li, Y. Ban, *Chem. Commun.*, 2013, **49**, 9140—9142.
22. X. Cheng, A. Zhang, K. Hou, *Dalton Trans.*, 2013, **42**, 13698—13705.
23. N. Hiyoshi, K. Yogo, T. Yashima, *Micropor. Mesopor. Mater.*, 2005, **84**, 357—365.
24. A. C. C. Chang, S. S. C. Chuang, M. Gray, *Energy Fuels*, 2003, **17**, 468—473.
25. R. Banerjee, H. Furukawa, D. Britt, C. Kobler, M. O´Keeffe, O. M. Yaghi, *J. Am. Chem. Soc.*, 2009, **131**, 3875—3877.
26. Y. Belmabkhout, G. D. Weireld, A. Sayari, *Langmuir*, 2009, **25**, 13275—13278.
27. J. Liu, P. K. Thallapally, B. P. McGrail, *Chem. Soc. Rev.*, 2012, **41**, 2308—2322.
28. A. Zhao, A. Samanta, P. Sarkar, R. Gupta, *Ind. Eng. Chem. Res.*, 2013, **52**, 6480—6491.

Received May 30, 2018;
in revised form July 16, 2018;
accepted July 31, 2018